Research Article

A Grid Fusion Lifting Surface and Its Flow Control Mechanism at High Angles of Attack

Fan Hua-yu,[1] Mi Bai-gang [ID],[2] Liu Han-yu,[3] and Yu Jing-yi[2]

[1]*AVIC Xi'an Aeronautics Computing Technique Research Institute, Xi'an 710065, China*
[2]*School of Aeronautics, Northwestern Polytechnical University, Xi'an, Shaanxi, China*
[3]*Beijing Institute of Astronautical Systems Engineering, Beijing 100076, China*

Correspondence should be addressed to Mi Bai-gang; mibaigang@163.com

A grid fusion lifting surface suitable for large subsonic angles of attack was designed. The influence of the grid position, grid diversion angle, and grid number on the aerodynamic performance of the grid fusion lifting surface under subsonic conditions was studied by numerical simulations. Based on the summary and analysis of the grid in the hypersonic state, the CFD numerical simulation method, which solves unsteady Reynolds averaged Navier-Stokes equations, was used to complete the research of the flow mechanism of the grid fin in the subsonic state. At low speed and subsonic conditions, the results show that the negative front grid fusion lift surface has better aerodynamic characteristics with a high angle of attack. Under subsonic conditions, the stall angle of attack of the front grid fusion lifting surface with a diversion angle of $20°$ increases by $16°$, and the maximum lift coefficient increases by 22.1% compared to that of the conventional flat wing. The number of grids has an insignificant effect on the aerodynamic performance of the grid fusion lifting surface at a large angle of attack.

1. Introduction

The grid wing is a multifaceted lift system composed of external grid frames and internal grid partitions [1, 2]. Due to its special polyhedral structure, it has excellent aerodynamic performance compared with the traditional flat wing, including enhanced lift performance for large angles of attack, little movement of the pressure center, and low hinge moment [3–6].

With the rapid development of aerospace technology in recent years, the application of grid fins as full-motion rudders and stable wing surfaces of rockets and missiles in the supersonic field has become more mature [7]. Many scholars and research institutions have performed aerodynamic research on grid fins. Chen studied the aerodynamic performance of grid fins with different grid thicknesses and leading edge shapes under supersonic conditions [8, 9], and the results demonstrated that the grid parameters significantly affected the lift-drag performance of the grid fin. Chen and

Deng [10] used the numerical simulation method to predict the roll damping derivatives of missiles with grid wings and flat wings in the supersonic state, and the results show that the efficiency of generating roll damping of a grid fin is much higher than that of a single fin. Yang and Zhang [11] proposed a new strategy for the optimization design of complex aerodynamic configurations, which obtained the optimal results of grid fins with a lower computational cost. Li et al. [12] proposed an improved circular-arc grid-fin configuration, which could effectively reduce the drag of grid fins at supersonic speeds. Huang et al. [13] studied the aeroelasticity of grid fins under transonic and supersonic conditions, and the results showed that the deformation of the grid fin reduced and reversed the hinge moment. Liu et al. [14] studied the aerodynamic heat of grid fins, and the influence of shock wave mutual interference on heat flux was analyzed in detail. Tripathi et al. [15] systematically studied the influence of the aspect ratio on the aerodynamic performance of grid fins through wind tunnel experiments.

Current studies on grid fins mostly focus on supersonic and hypersonic aerospace applications and rarely involve the aviation field, mainly due to the considerable drag caused by the multisided structure of grid fins. However, the grid fin's unique large angle of attack is a desirable advantage to improve the subsonic aircraft performance. The problem of excessive drag must be solved to apply grid fins to aircraft. At present, the drag reduction methods of grid fins mainly include sweeping the overall grid fin back, sweeping the local grid fin back, reducing the number of grids, and changing the cross-sectional shape of grid baffles [16–22]. The conventional drag reduction method can reduce the grid fin's aerodynamic drag, but the multisided structure of the grid fin is unchanged, and the optimized grid fin still has larger aerodynamic drag than the traditional single fin [23].

This paper innovatively proposes a grid fusion lifting surface scheme suitable for subsonic and large angles of attack based on flow control technology design. The numerical simulation method is used to study the influence of grid attributes, such as the grid position, grid diversion angle, and grid number, on the aerodynamic performance of the grid fusion lifting surface under subsonic conditions. The purpose of this paper is to explore a new large angle of attack flow-control scheme for aeronautical aircraft and improve its comprehensive performance.

2. Design of the Grid Fusion Lifting Surface

2.1. Analysis of the Aerodynamic Performance of Conventional Grid Fins. In general, the structural types of grid fins are mainly truss (frame) and cellular type. The cellular grid fins are further divided into straight and oblique cellular grid fins. Schematic diagrams of three different structural types of grid fins are presented in Figure 1.

At supersonic speed, the grid wing has some advantages that the traditional flat wing does not have, including better lift performance for large angles of attack, minimal pressure center movement, low hinge moment, and easier folding and mounting performance.

The main disadvantage of grid fins under subsonic conditions is the large aerodynamic drag. The multifaceted structure leads to a larger wetting area of the grid fin and causes substantial friction drag. In the transonic state, shock waves are generated inside the grid structure and initiate considerable shock drag. Furthermore, the grid fin has worse lift-drag performance than the traditional flat wing in the subsonic state.

The aerodynamic performance of grid fins is more sensitive to the flow performance between grid partitions, which mainly depends on the far-field velocity. Figure 2 displays a schlieren diagram of the supersonic flow field between grid partitions with different incoming flow velocities. As shown in Figure 2(a), when the inlet Mach number is subsonic, positive shock waves are generated inside the grid separator, which increases the grid wing resistance. Currently, the corresponding Mach number of incoming flow is called the first critical Mach number M_{kp1}. Figure 2(b) illustrates a schlieren diagram of the shock waves inside the grid when M_{kp1}

$< Ma < M_{kp2}$. Supersonic flow appears near the grid outlet with increasing Mach number and forms a mesh shock near the grid outlet. When the flow velocity reaches a low supersonic speed, positive shock waves appear in the front section of the grid fin. The shock wave is attached to the leading edge of the grid fin when the inlet Mach number reaches M_{kp2}, which is called the second critical Mach number. Figure 2(c) shows a schlieren diagram of the shock waves inside the grid when $Ma = M_{kp2}$. In this case, the drag of the grid wing sharply increases. These phenomena explain the poor drag performance of the grid fin in subsonic and transonic conditions.

Figure 2(d) presents a schlieren diagram of the shock waves inside the grid when $M_{kp2} < Ma < M_{kp3}$. At this time, oblique shock waves inside the grid appear many times between grid partitions. When the Mach number increases and when the oblique shock wave in the grid is not reflected between the grid panels, the incoming Mach number is called the third critical Mach number M_{kp3}. Figures 2(e) and 2(f) show schlieren diagrams of the shock waves inside the grid when $Ma = M_{kp3}$ and $Ma > M_{kp3}$. When the Mach number of incoming flow exceeds M_{kp3}, there is no reflection of the shock wave inside the grid partition, and there is no interference between each grid partition. At this time, the grid fin has better lift performance.

2.2. Design of the Grid Fusion Lifting Surface. The increase in grid fin drag under subsonic and transonic conditions is due to the more significant friction drag caused by the grid fin's larger wetted area and the greater shock drag induced by the shock wave inside the grid partition. The drag reduction mechanism of the conventional drag reduction methods, such as sweeping the overall grid fin back, sweeping the local grid fin back, reducing the number of grids, and changing the cross-section shape of the grid baffle, is mainly to improve the airflow congestion of grid fins by changing the configuration of grid fins. The optimized grid fin drag is reduced, but the conventional drag reduction method does not fundamentally change the multifaceted structure of the grid fin. Therefore, the aerodynamic drag of the grid fin cannot be greatly reduced.

The conventional grid fin cannot be directly applied in the subsonic state and aviation field due to its poor drag performance. Based on flow control technology, the grid fusion lifting surface was designed by embedding a grid structure on a single wing. Compared with conventional grid fins, this scheme has fewer grid partitions and a larger grid width chord. This scheme combines the advantages of the traditional grid and flat wing, which effectively reduces the grid structure drag and significantly improves the lifting surface performance at large angles of attack under subsonic conditions. Figure 3 shows the global view and typical spanwise section view of the grid fusion lifting surface in the form of an embedded grid.

The inherent properties of the grid structure directly affect the aerodynamic performance of the grid fusion lifting surface, which mainly includes the grid position, grid diversion angle, and the number of grids. The grid diversion angle and grid position directly affect the flow performance of the
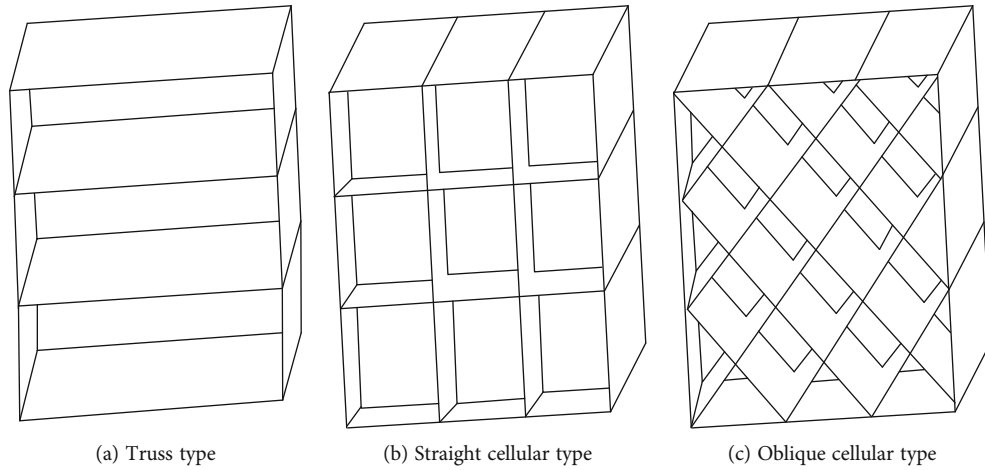
(a) Truss type   (b) Straight cellular type   (c) Oblique cellular type

FIGURE 1: Schematic diagram of grid wing with different structural forms.
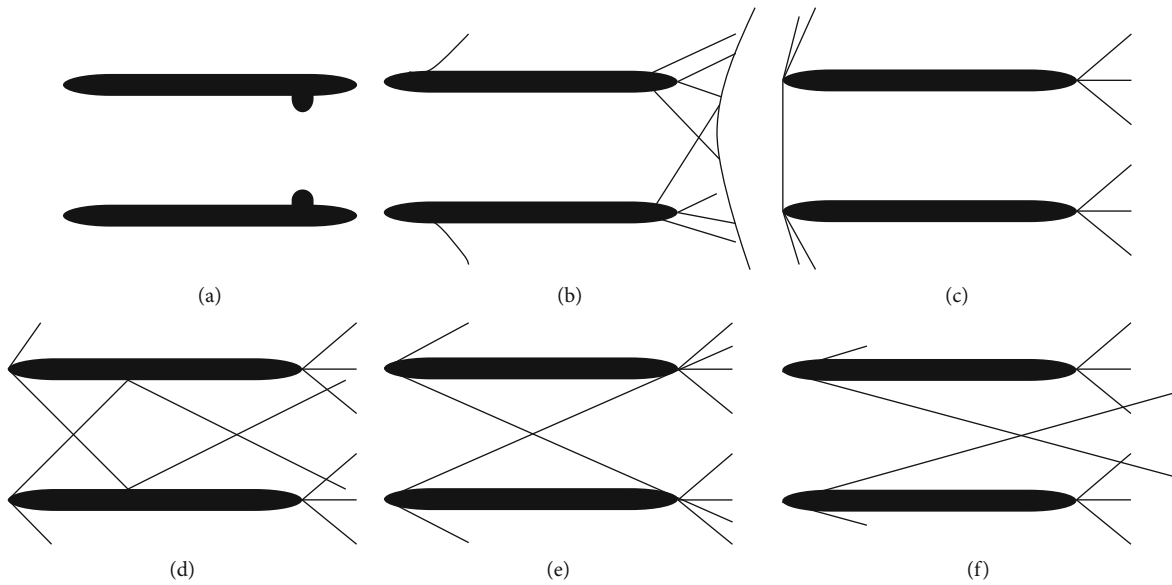

(a)   (b)   (c)

(d)   (e)   (f)

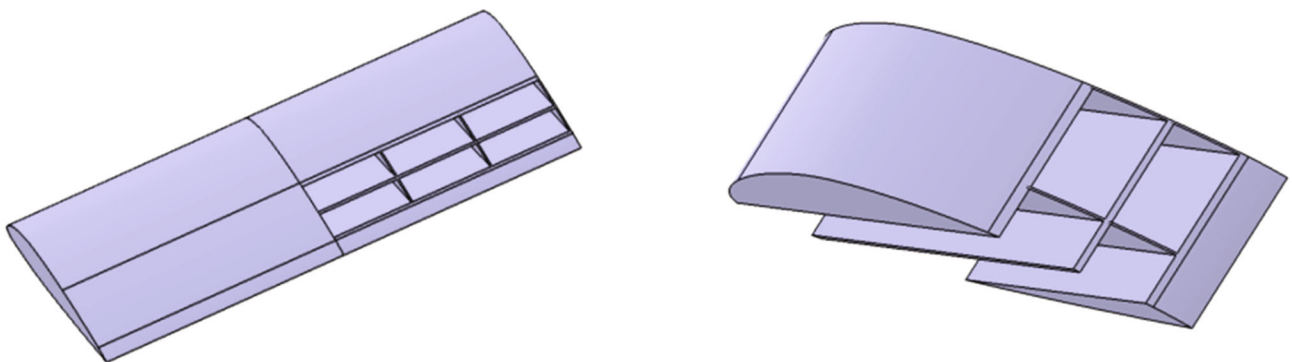FIGURE 2: Flow state between grid wing partitions with different critical Mach numbers.

FIGURE 3: Schematic diagram of grid fusion lifting surface.

grid fusion lifting surface, and the number of grids affects the actual lift area of the grid fusion lifting surface. In the following chapters, we study the influence law of the inherent design parameters of the grid fusion lifting surface on the aerodynamic performance, and the application environment of the grid fusion lifting surface is clarified. Exploratory research is performed for engineering applications of grid fusion lifting surfaces.
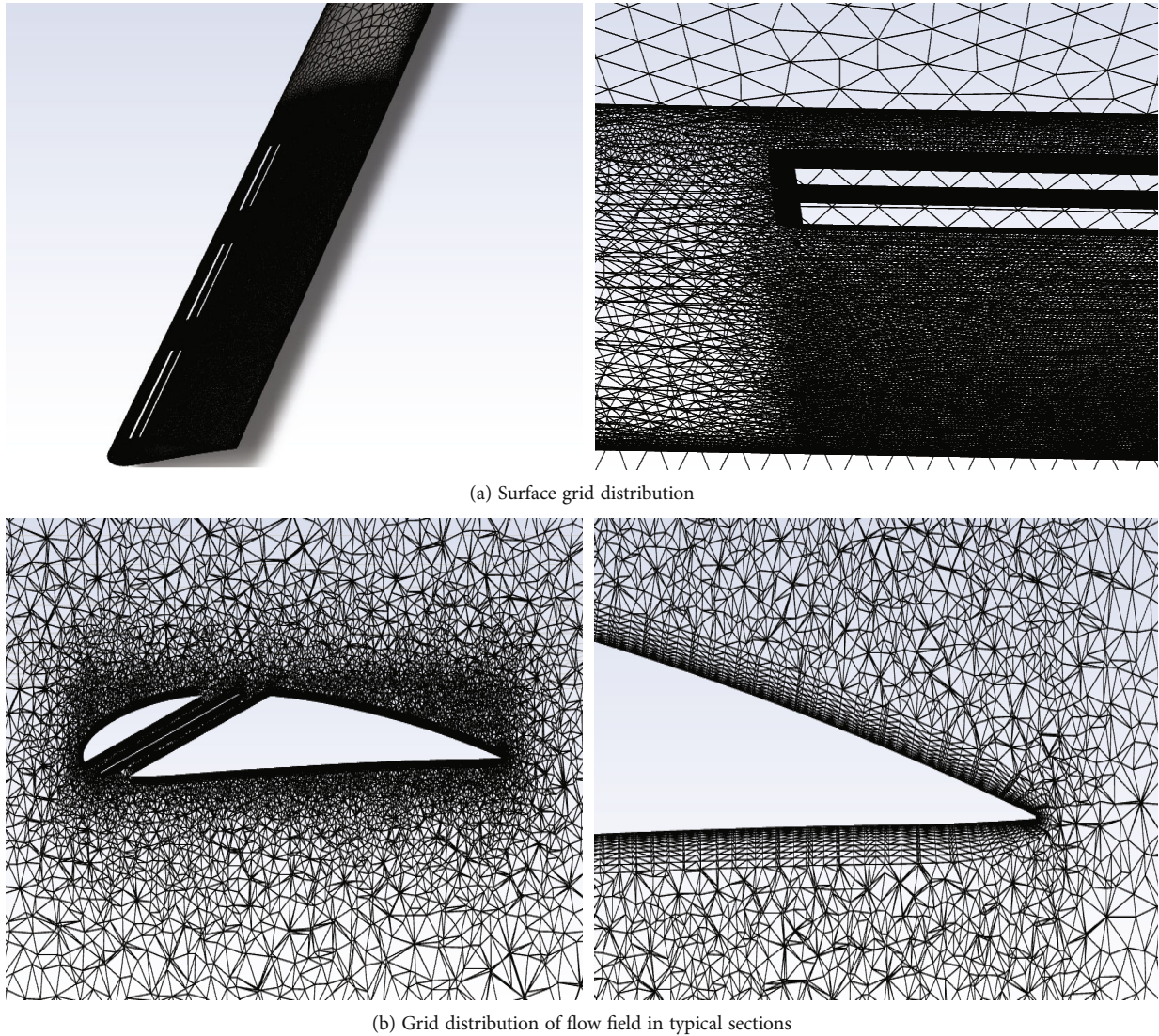
(a) Surface grid distribution

(b) Grid distribution of flow field in typical sections

FIGURE 4: Computational domain grid of grid fusion lifting surface with the diversion angle of 20° and grid number of 2.

3. Calculation Method and Verification

3.1. Governing Equation. The numerical simulation in this paper is based on the three-dimensional unsteady Reynolds averaged N-S equation:

$$\frac{\partial Q}{\partial \tau} + \frac{\partial F}{\partial \xi} + \frac{\partial G}{\partial \eta} + \frac{\partial H}{\partial \zeta} = \frac{1}{\text{Re}} \left(\frac{\partial F_v}{\partial \xi} + \frac{\partial G_v}{\partial \eta} + \frac{\partial H_v}{\partial \zeta} \right) \quad (1)$$

where Q is a conserved variable vector; F, G and H are inviscid flux vectors; F_v, G_v and H_v are viscous flux vectors. The discrete equation was established based on the finite volume method, and the second-order upwind difference scheme was adopted to solve the discrete difference equations. The explicit time advance solution algorithm based on density was applied to solve the discrete difference equations. The shear stress turbulence model ($k - \omega$ SST) [3, 24] was employed in the turbulence model. The turbulence model was selected based on two considerations: high computational efficiency; the transport of turbulent shear stress is considered to avoid overpredicting the eddy current viscosity.

3.2. Computing Grids. Due to the complexity of the grid structure, the flow field of the grid fusion lifting surface is discretized with unstructured grids with ICEM CFD software. An appropriate refining grid was performed in places with large flow gradients, such as grid plates and holes, and the total number of grids was approximately 2.5-3.5 million. Figure 4 shows the surface and typical cross-section grid distribution of the front section grid fusion lifting surface with a diversion angle of 20°.

Since we will use the $k - \omega$ SST model to simulate the aerodynamic performance of the configurations, the calculating grid should fit the requirement of the turbulence

(a) Surface mesh distribution of delta wings

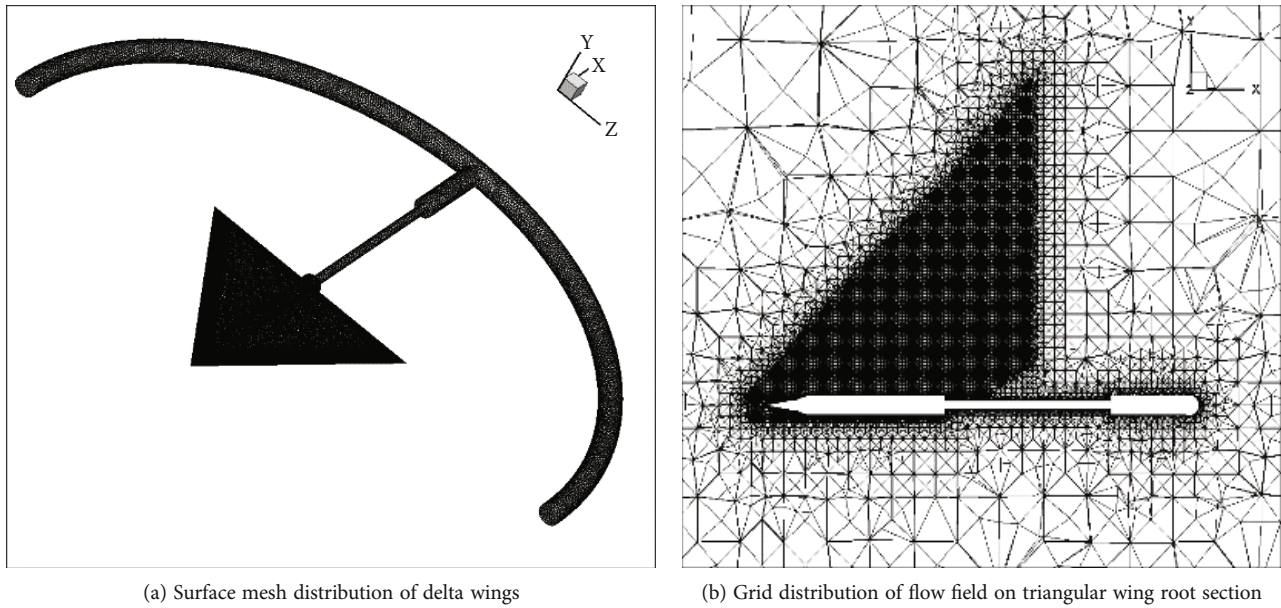(b) Grid distribution of flow field on triangular wing root section

FIGURE 5: Delta wing meshing strategy.

model. In ANSYS Fluent software, the relation between grid and turbulence model mainly focuses on the y+ of the boundary mesh, which implies that the height of the first layer in the boundary mesh will be combined with the turbulence model to determine the calculation accuracy of the flow field. For the $k - \omega$ SST model, we can define a reasonable value of y+ to improve the accuracy. In this study, we generate a high-quality mesh with y+ $\approx$1 to satisfy the turbulence model. Moreover, the mesh has been refined around the leading edge, trailing edge and backward area of the configuration to capture the flow characteristics as precisely as possible with the $k - \omega$ SST model.

3.3. Verification of Calculation Method. Since the calculation involves large angles of attack, the calculation method is initially verified. Generally, more accurate models are required to simulate vortex system changes at higher angles of attack. Such as DES and LES. However, these methods are computationally expensive. This paper aims to study the scheme's feasibility, so the two-equation $k - \omega$ SST model based on RANS is used to complete the calculation. In this section, two standard models are used to verify the numerical method.

First, the flow field of a delta wing with a sweep angle of 60° is numerically calculated, and the simulation results are compared with experimental results [25]. According to the experimental data of the delta wing, the selected calculation states are as follows: the inlet flow velocity is 30 m/s; the atmospheric pressure is 101,325 Pa; the angle of attack is 0°, 10°, 30°, and 50°; the ambient temperature is 288 K. The flow field of the delta wing is discretized with unstructured grids, and the leeward region of the delta wing is locally refined. The number of grids is approximately 8 million. Figure 5 shows the grid distribution of the delta wing computing domain.

Figure 6 compares the numerical calculation results of the delta wing with the experimental results of Nanjing University of Aeronautics and Astronautics (NUAA) and Harbin Institute of Technology (HIT) [26]. The findings suggest that when the angle of attack is small, the numerical simulation results of the delta wing's normal force coefficient are consistent with the experimental values. When the angle of attack exceeds 30 degrees, the CFD value of the delta wing is smaller than the experimental value, but the numerical value is similar to the experimental value in the trend. There are some differences in experimental values of the delta wing pitching moment that varies with the angle of attack between Nanjing University of Aeronautics and Astronautics and Harbin Institute of Technology. The numerical simulation results of the delta wing pitching moment in this paper are close to the experimental results of the NUAA.

In addition, to verify the accuracy of the numerical simulation method to solve the problem of grid wing aircraft, a numerical calculation is proposed for the grid tail missile standard model. According to the experimental data of the grid tail missile, the selected calculation states are as follows [27]: the Mach number is 0.5, and the Reynolds number based on the maximum diameter of the grid tail missile is 2.27×10^7. Figure 7 shows the grid distribution on the surface of the calculation domain of the grid tail missile. The flow field of the grid tail missile is discretized with the unstructured grid, the key calculation area grid is locally refined, and the number of grids is approximately 10 million.

Figure 8 compares the CFD numerical calculation results and the experimental data [27] of the normal force coefficient of the raster tail missile wing body assembly, which shows basic consistency with each other around the entire range of angles of attack. In some special cases, the lift coefficient is slightly higher and the drag coefficient is slightly

(a) The variation trend of delta wing normal
force coefficient with angle of attack

(b) The variation trend of delta wing pitching
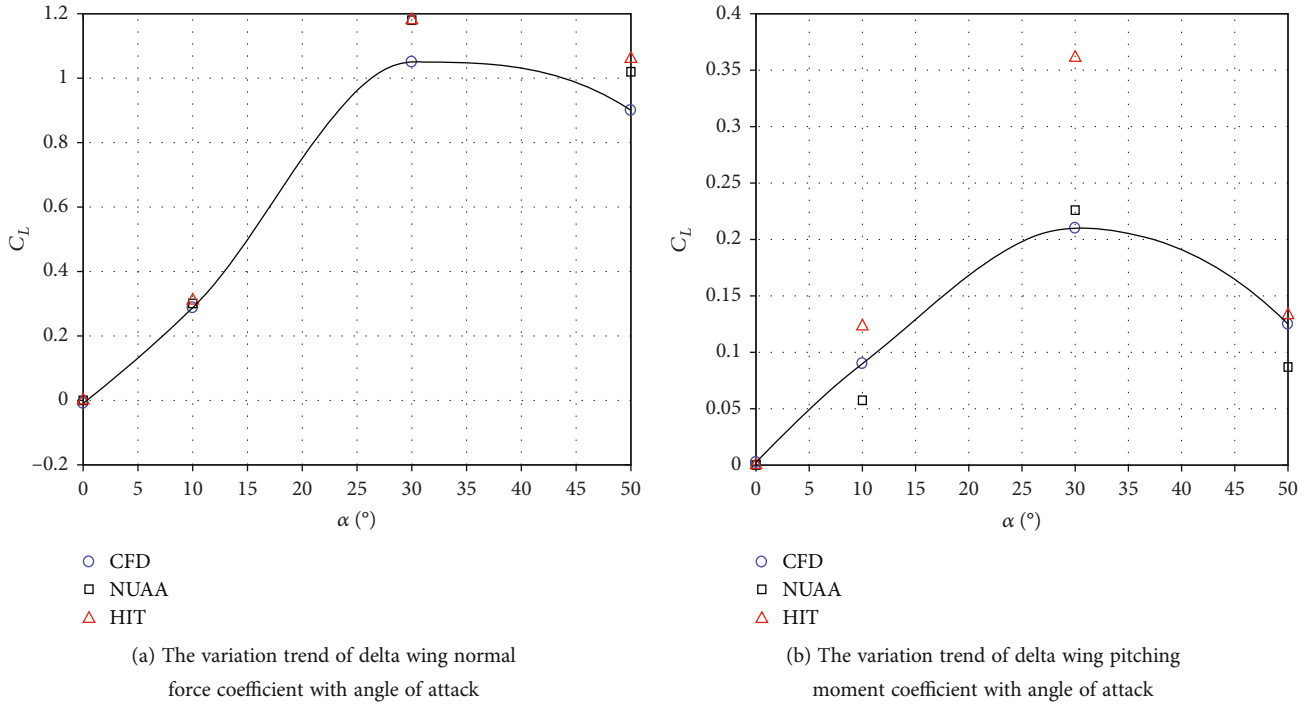moment coefficient with angle of attack

FIGURE 6: Comparison of experimental results and numerical results of delta wing 1.
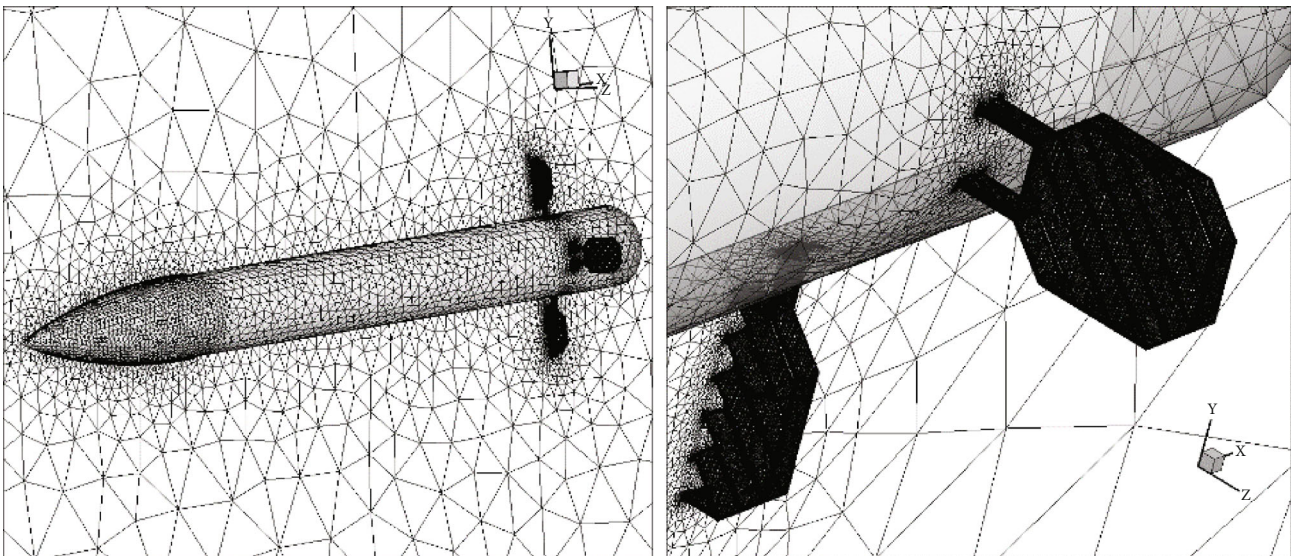

FIGURE 7: Grid tail meshing strategy.

lower, which may be because the model cannot fully capture the flow field details of these models.

In summary, the numerical calculation method in this paper can accurately describe the aerodynamic performance of aircraft at small angles of attack and approximately describe the basic aerodynamic performance of grid wing aircraft at large angles of attack. Therefore, the simulation can satisfy the requirements of the research on the aerodynamic performance of the raster fusion lift surface.

4. Analysis of the Aerodynamic Performance and Flow Field Mechanism of the Grid Fusion Lift Surface at Large Angles of Attack

Numerical simulations were performed on the aerodynamic performance of the grid fusion lifting surface with different inherent attributes of the grid to explore the application environment of the grid fusion lifting surface under the
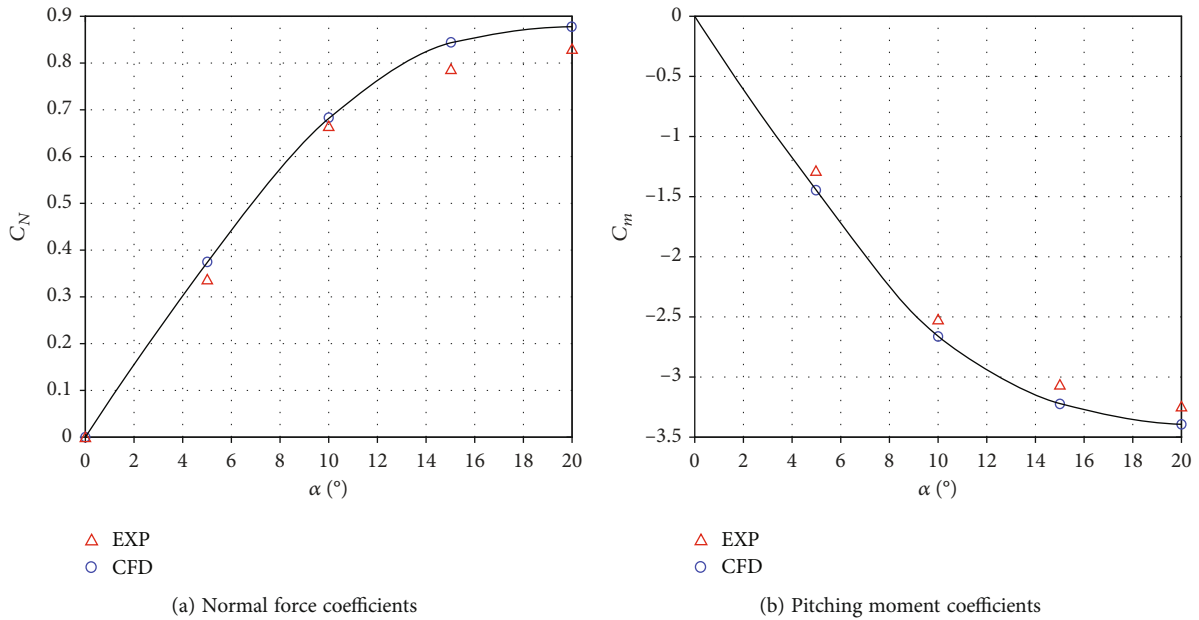
(a) Normal force coefficients

(b) Pitching moment coefficients

FIGURE 8: The CFD numerical calculation and experimental results of the grid tail missile.

(a) Front grid fusion lifting surface

(b) Central grid fusion lifting surface
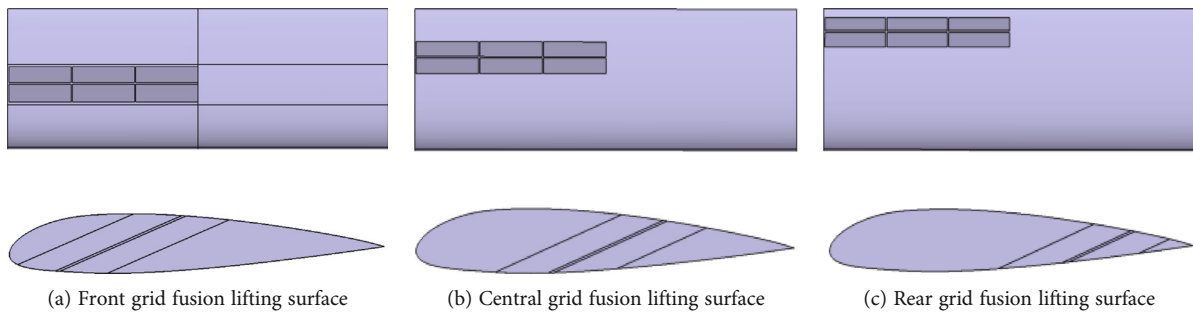
(c) Rear grid fusion lifting surface

FIGURE 9: Calculation model of grid fusion lifting surface with different grid positions1.

subsonic state. The influence law of the grid position, grid diversion angle, and grid number on the aerodynamic performance of the grid fusion lifting surface was studied, and the optimal structure form of the grid fusion lifting surface was obtained.

The grid position directly affects the flow performance of the grid fusion lifting surface and aerodynamic performance. The aerodynamic performance of the grid fusion lifting surface with different grid positions with a diversion angle of $20°$ and two grid numbers was studied to examine the influence of grid position on the aerodynamic performance of the grid fusion lifting surface. Figure 9 shows the calculation model of the grid fusion lift surface with different grid positions.

The diversion angle is the included angle between the strings of the grid structure and the wing strings, as shown in Figure 10. The diversion angle mainly affects the flow quality around the exhaust port of the grid structure and aerodynamic performance of the lift surface with a large angle of attack. The aerodynamic performance of the grid
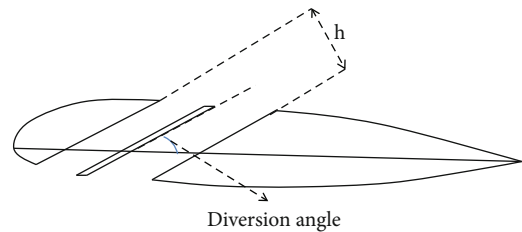

FIGURE 10: Diagram of diversion angle2.

fusion lifting surface with different diversion angles was studied to investigate the influence of the diversion angle on the aerodynamic performance of the grid fusion lifting surface. Figure 11 shows the calculation model of the front grid fusion lifting surface with different diversion angles.

The number of grids is the number of grids in the chordal direction of the grid fusion lifting surface, which
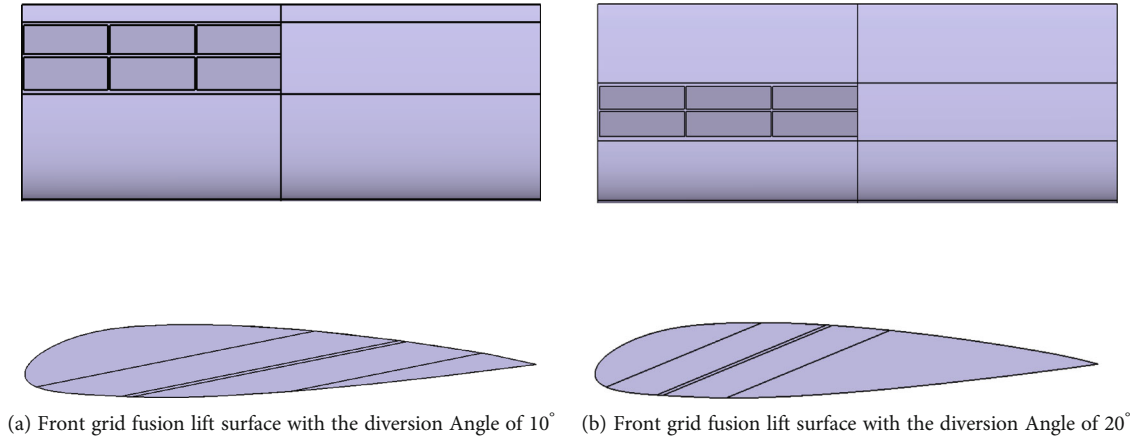
(a) Front grid fusion lift surface with the diversion Angle of 10°   (b) Front grid fusion lift surface with the diversion Angle of 20°

Figure 11: Calculation model of grid fusion lifting surface with different diversion angles3.

(a) Grid fusion lifting surface with grid number of 1   (b) Grid fusion lifting surface with grid number of 2

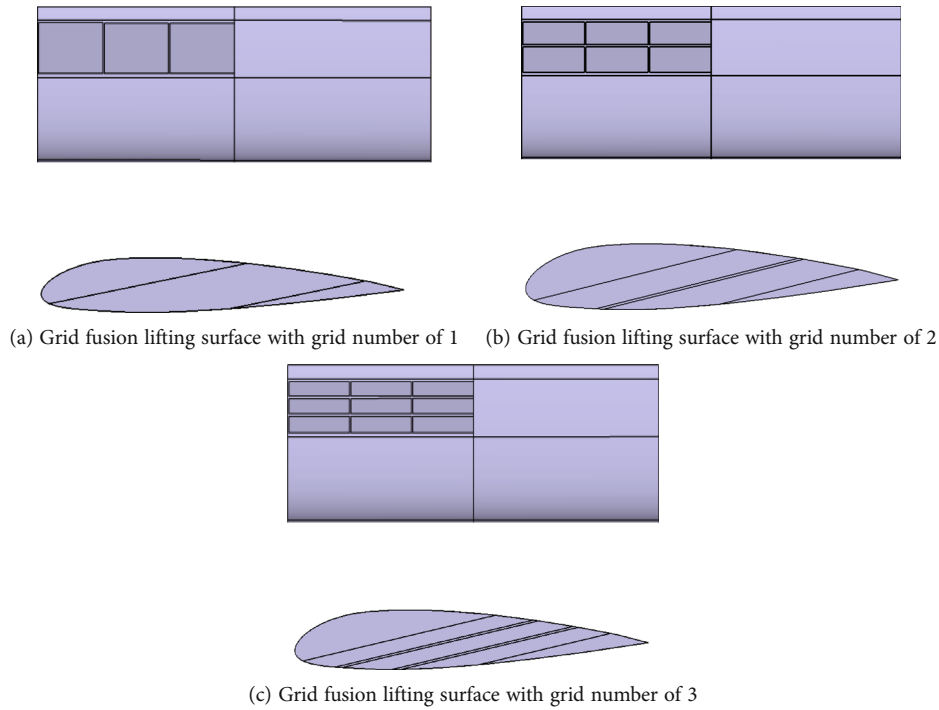(c) Grid fusion lifting surface with grid number of 3

Figure 12: Calculation model of lifting surface with different grid numbers4.

directly affects the actual lift area of the grid fusion lifting surface. In the conventional research of grid fins, more grids correspond to a larger lifting area of grid fins, better lifting performance of grid fins, and worse drag performance. In this section, the influence law of the number of grids on the aerodynamic performance of the grid fusion lifting surface under the subsonic state is studied. Figure 12 shows the calculation model of the grid fusion lifting surface with different grid numbers.

The numerical boundary conditions include far-field boundaries, nonslip wall boundaries, and symmetric surface boundaries. The calculation state is as follows: inlet Mach number: $Ma = 0.6$; angle of attack: $\alpha = 0° - 36°$ (calculation interval: $4°$); reference height: sea level; reference length: L $= 0.2$m; reference area: $S = 0.12$m^2; Reynolds number based on the average aerodynamic chord length: Re $= 2.8 \times 10^6$.

4.1. Validation of the Mesh and Time Step Size Independencies. We first validate the mesh and time step size independencies because the simulations will be proposed by unsteady calculation. The lifting surface with central grid fusion is chosen to present the analysis. The original mesh with 3 million nodes has been dynamically refined or unrefined to generate 1.5, 2, 3.5, and 4 million nodes to testify to the effect of the mesh on the aerodynamics of the configuration. The time step size in the simulation is defined as 0.001 s. The mesh has been changed mainly near the backward area of the surface, while the first heights of the mesh
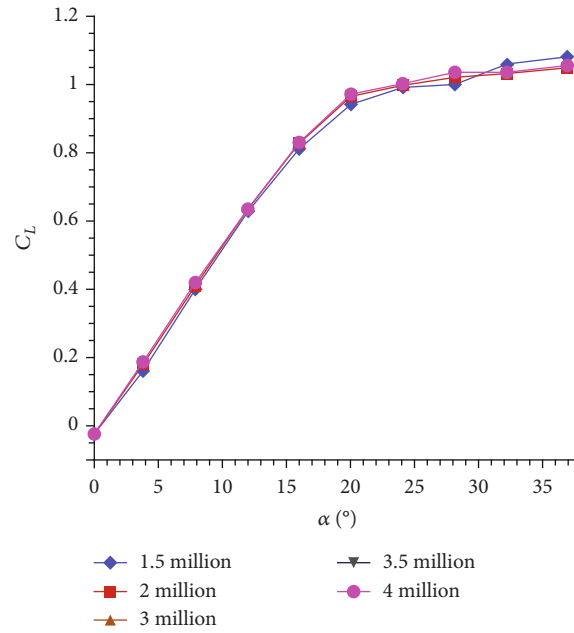
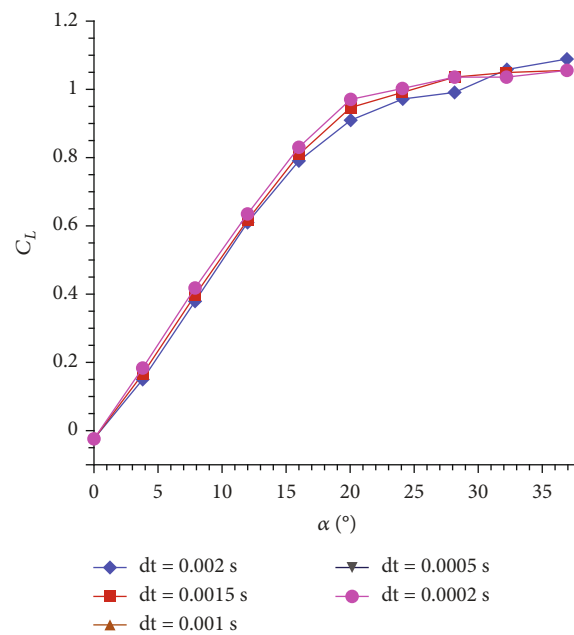FIGURE 13: Lifts of different mesh quantities.

FIGURE 14: Lifts of different time step sizes.

in the boundary layer are the same in these cases. Figure 13 shows the lift results with different mesh quantities. The mesh with 3 million nodes can clearly obtain the basically convergence aerodynamic performance, so we will use a similar mesh generating method to propose a further simulation.

The calculations in this study involve flow separations at high angles of attack; thus, we use an unsteady method to capture the dynamic effects. Although the $k - \omega$ SST model cannot accurately describe the aerodynamic performance at a high angle of attack, some medium flow separations can

be identified. We compare different time step sizes $\Delta t = 0.0002s, 0.0005s, 0.001s, 0.0015s, 0.002s$ in the unsteady calculations to validate the time step size independency, and the lifts are shown in Figure 14. The time step size influences the stability and convergence of the solutions, and a smaller time step size will lead to a more stable calculation; however, the convergence will be delayed. Figure 14 indicates that smaller values below 0.0015 s can obtain similar lift results at all angles of attack, so the remaining solutions will be proposed with a certain time step size of $\Delta t = 0.001s$.
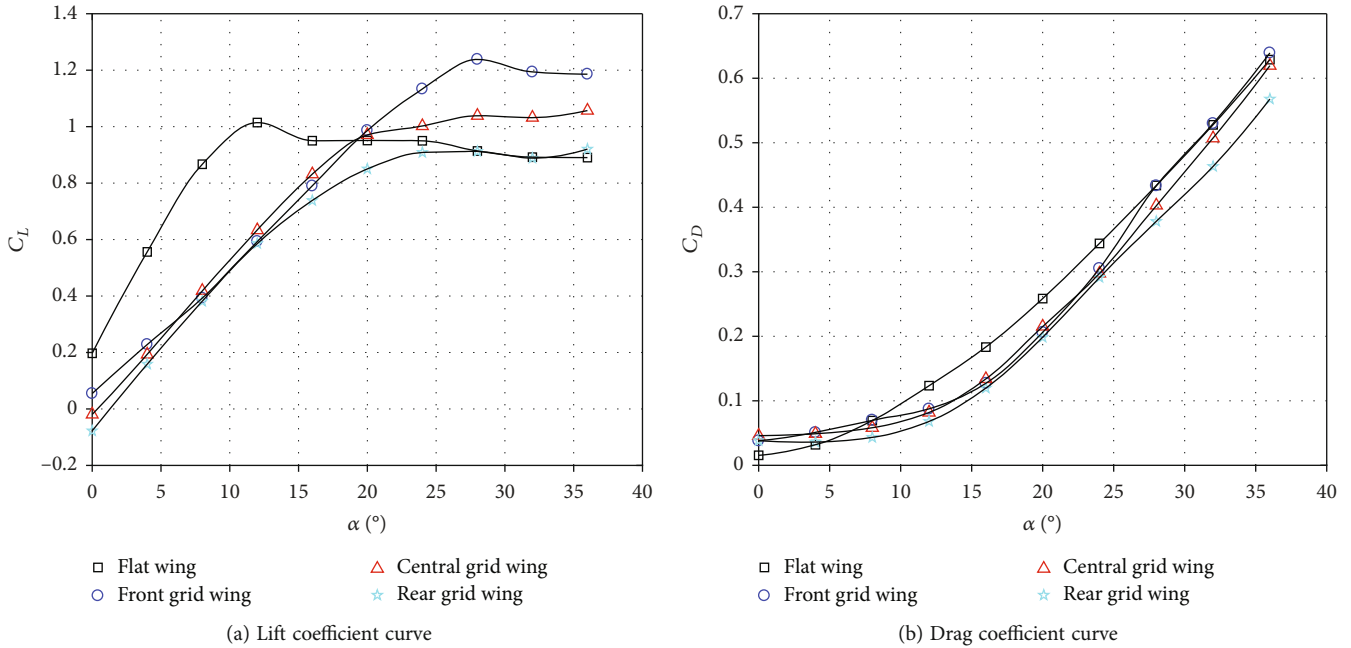
(a) Lift coefficient curve

(b) Drag coefficient curve

FIGURE 15: The lift coefficient and drag coefficient curves of the grid fusion lifting surface with different positions ($Ma = 0.6$).

4.2. Influence of the Grid Position on the Aerodynamic Performance of the Grid Fusion Lifting Surface at Large Angles of Attack.

Figure 15(a) displays the lift coefficient curves of the grid fusion lifting surface with different grid positions under subsonic conditions. The results imply that the front grid fusion lifting surface has the best lift performance compared with the flat wing, central grid fusion lifting surface, and rear grid fusion lifting surface under the condition of subsonic flow and large angles of attack. Compared with the conventional flat wing, the stall angle of attack of the front grid fusion lifting surface with a 20° diversion angle and 2 grids increases by 16°, and the maximum lift coefficient increases by 22.1%. When the angle of attack is less than 20 degrees, the grid fusion lifting surface with different grid positions has worse lifting performance than the flat wing. Figure 15(b) presents the drag coefficient curves of the grid fusion lifting surface with different grid positions under subsonic conditions. The results show that when the angle of attack is 20-28°, the front grid fusion lifting surface has a lower drag coefficient than the traditional flat wing and when the angle of attack is greater than 28°. The drag coefficient of the front grid fusion lifting surface is less different from that of the traditional flat wing. Under the condition of a large angle of attack, the central grid fusion lifting surface and rear grid fusion lifting surface have less drag than the front grid fusion lifting surface.

Figure 16 shows the fluid streamline diagrams of a typical section of a flat wing and grid fusion lifting surface with different positions under the condition of a Mach number of 0.6 and an attack angle of 28°. The results show that the flat wing completely stalls under this condition. The airflow discharged from the front grid structure significantly reduces the degree of airflow separation on the lifting surface. A small separation vortex appears on the upper surface of the front edge. The flow dead water area on the upper surface of the trailing edge is confined to the area near the wing surface, and no larger vortex separation is generated. Therefore, the front grid fusion lifting surface at a large angle of attack has significantly better lift performance than the conventional flat wing. The separation degree of airflow on the upper surface of the central grid fusion lifting surface and rear grid fusion lifting surface remains significant, and the stall resistance ability is lower than that of the front grid fusion lifting surface.

Figure 17 exhibits the pressure coefficient diagram of typical sections of the grid fusion lifting surface with different positions in the subsonic state with an angle of attack of 28°. The pressure coefficient diagram of the grid fusion lifting surface presents three closed loops, which correspond to the pressure coefficient of the front part of the grid fusion lifting surface, the grid partition, and the rear portion of the grid fusion lifting surface. The results show that a negative pressure peak appears on the upper surface of the front grid fusion lifting surface because the high-energy airflow discharged from the grid outlet resists the separation of the airflow on the upper surface of the trailing edge of the lifting surface. Moreover, the curvature of this area is large, which causes a significantly lower pressure in this area than the traditional single-wing, which is of great significance for improving the lift performance of the lift surface under the condition of a large angle of attack. The lifting surface of the grid fusion type in the middle and rear sections is weak in resisting the air separation, and the negative pressure peak generated by the surface of the lifting surface is not apparent.

A negative pressure sag appears in front of the lower surface of the grid fusion lifting surface due to the accelerated flow rate of the airflow in the grid and the large curvature in this area. The decrease in pressure on the lower surface
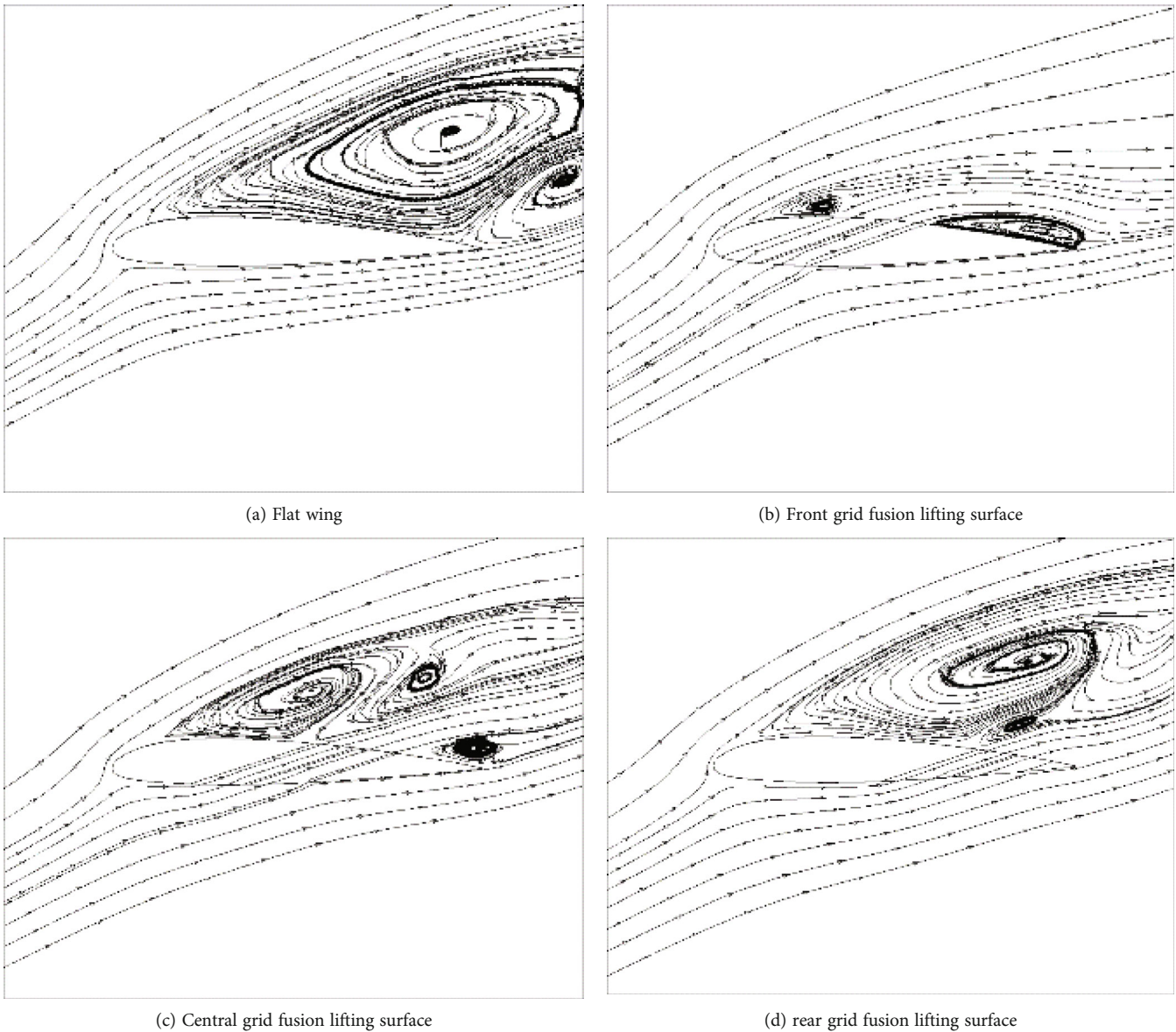
(a) Flat wing

(b) Front grid fusion lifting surface

(c) Central grid fusion lifting surface

(d) rear grid fusion lifting surface

Figure 16: Fluid streamline diagrams of grid fusion lifting surface with different grid Position ($Ma = 0.6\alpha = 28°z/b = 0.75$).

results in the loss of lift on the grid fusion lifting surface. When the grid is closer to the trailing edge, the negative pressure sag on the lower surface of the grid fusion lift surface is more significant, which indicates more serious lift loss. Therefore, the front grid fusion lifting surface has significantly better lift performance than the central grid fusion lifting surface and rear grid fusion lifting surface under the condition of a large angle of attack.

The grid position significantly affects the degree of airflow separation and the distribution of the lift surface pressure coefficient, which directly affects the aerodynamic performance of the grid fusion lift surface at a high angle of attack. When the grid is closer to the leading edge, the stall angle of attack of the grid fusion lifting surface increases, and the lift performance improves under the condition of a large angle of attack.

4.3. Influence of the Grid Diversion Angle on the Aerodynamic Performance of the Grid Fusion Lifting Surface at Large Angles of Attack.
Figure 18(a) shows the lift coefficient curve of the flat wing and grid fusion lifting surface with diversion angles of 10° and 20°. The results prove that a larger diversion angle corresponds to a larger stall angle of attack and a larger maximum lift coefficient of the grid fusion lifting surface. When the diversion angle is small, the stall angle of attack and maximum lift coefficient of the grid fusion lifting surface are minor, but the minimum angle of attack to increase the lift force is relatively small. Figure 18(b) shows the drag coefficient curve of the flat wing and grid fusion lifting surface with diversion angles of 10° and 20°. The results show little difference in the drag coefficient of the lifting surface with diversion angles of 10° and 20° for a large angle of attack. A larger diversion angle
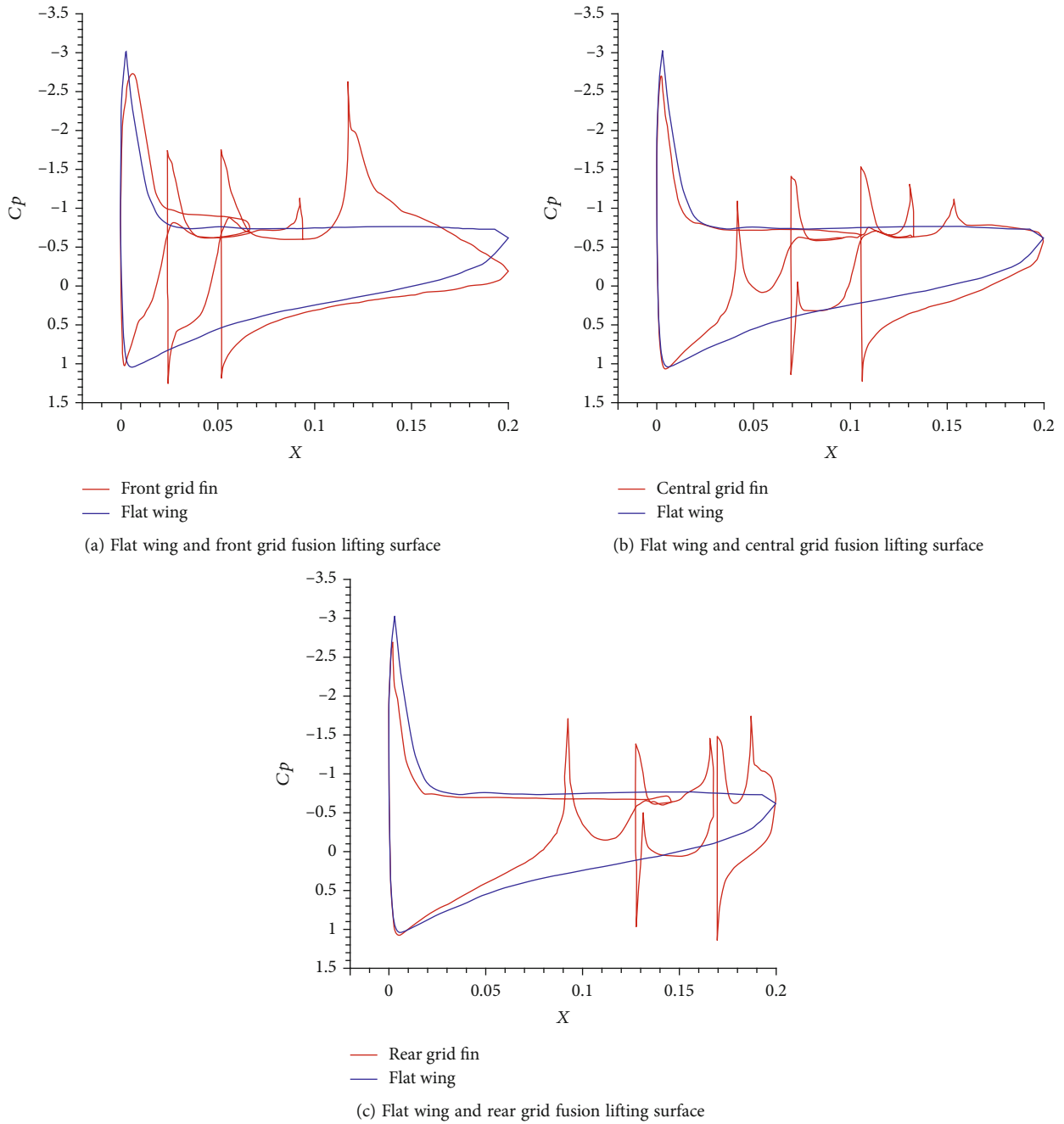
(a) Flat wing and front grid fusion lifting surface

(b) Flat wing and central grid fusion lifting surface

(c) Flat wing and rear grid fusion lifting surface

Figure 17: Pressure coefficient diagram of flat wing and grid fusion lifting surface with different grid Position ($Ma = 0.6 \alpha = 28° z/b = 0.75$).

corresponds to a greater drag of the grid fusion lifting surface under the condition of a large angle of attack.

Figures 19 and 20 show typical section fluid streamline diagrams of the flat wing and grid fusion lifting surface with diversion angles of 10° and 20° under subsonic conditions and a large angle of attack. The results show that when the angle of attack is 16°, airflow separation does not occur on flat wings and grid fusion lifting surfaces with diversion angles of 10°. Airflow separation occurs on the upper surface of the grid fusion lifting surface with a diversion angle of 20°. Therefore, a larger diversion angle corresponds to a smaller

attack angle of airflow separation on the lifting surface. As a result, when the angle of attack is less than 24°, the grid fusion lifting surface with a diversion angle of 10° has relatively better lift performance. When the angle of attack reached 28°, the flat wing significantly stalls, but the grid fusion lifting surface with a diversion angle of 20° can still resist airflow separation. Therefore, the grid fusion lifting surface with a diversion angle of 20° has a relatively larger stall angle of attack and the maximum lift coefficient.

Under subsonic conditions, the grid diversion angle greatly influences the lift performance of the grid fusion
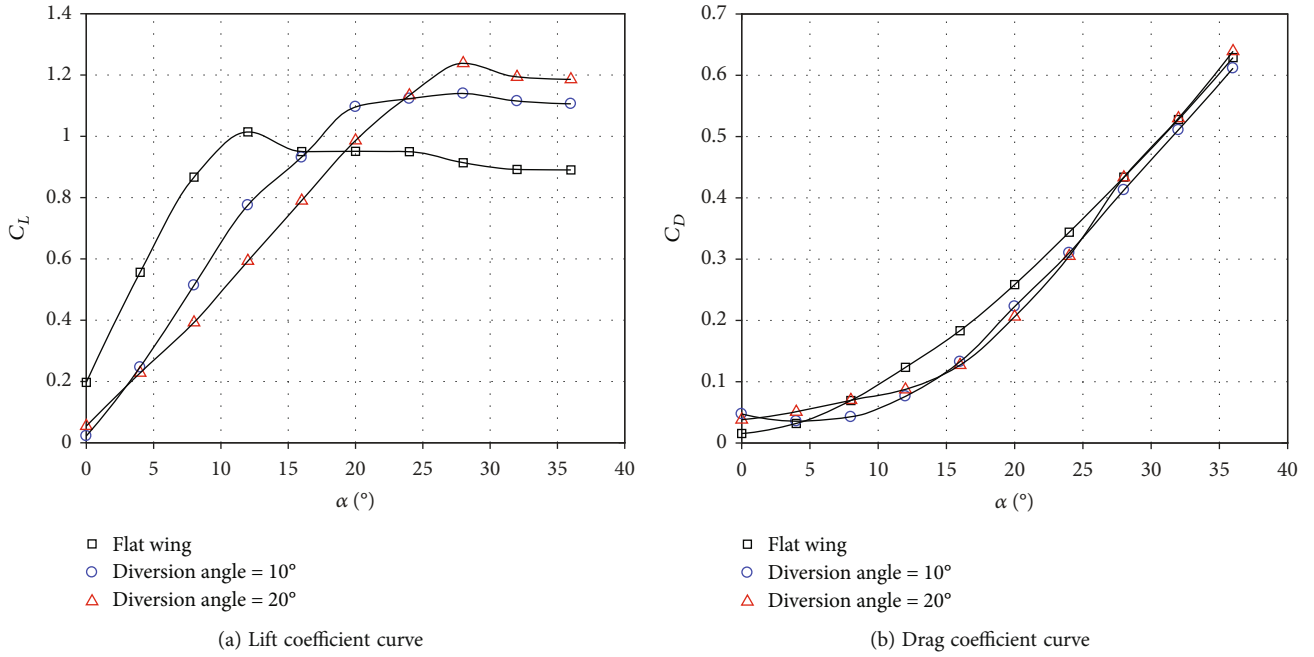
(a) Lift coefficient curve

(b) Drag coefficient curve

FIGURE 18: The lift coefficient and drag coefficient curves of the grid fusion lifting surface with different diversion angles ($Ma = 0.6$).

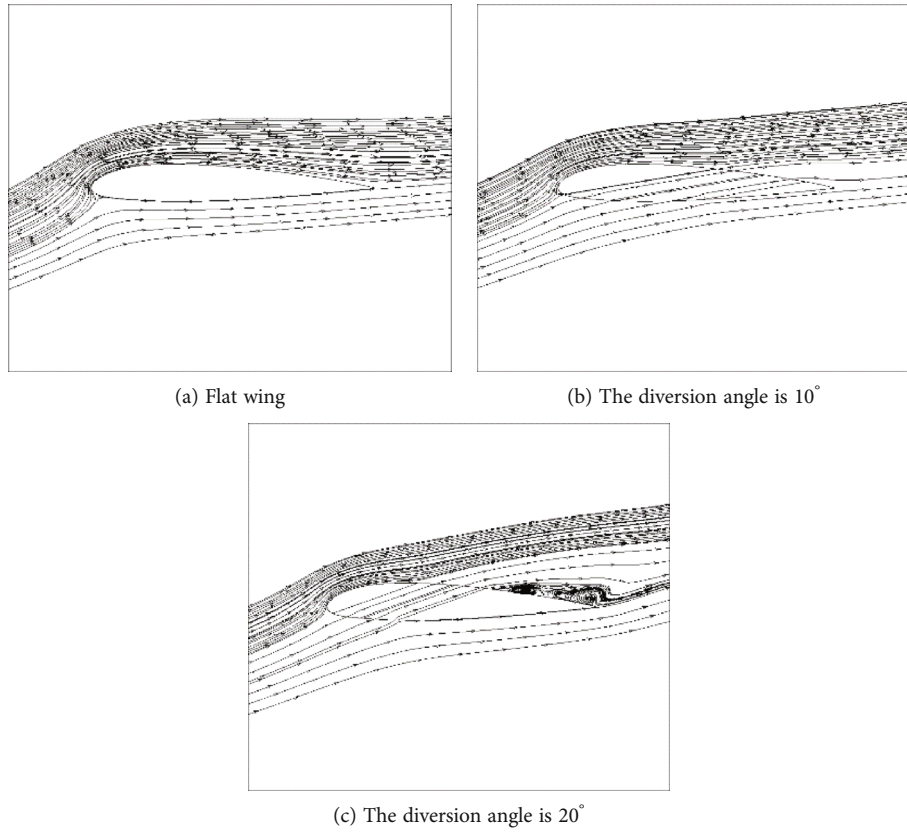(a) Flat wing

(b) The diversion angle is $10°$

(c) The diversion angle is $20°$

FIGURE 19: Fluid streamline diagrams of grid fusion lifting surface with different diversion angle ($Ma = 0.6 \, \alpha = 16° \, z/b = 0.75$).

(a) Flat wing

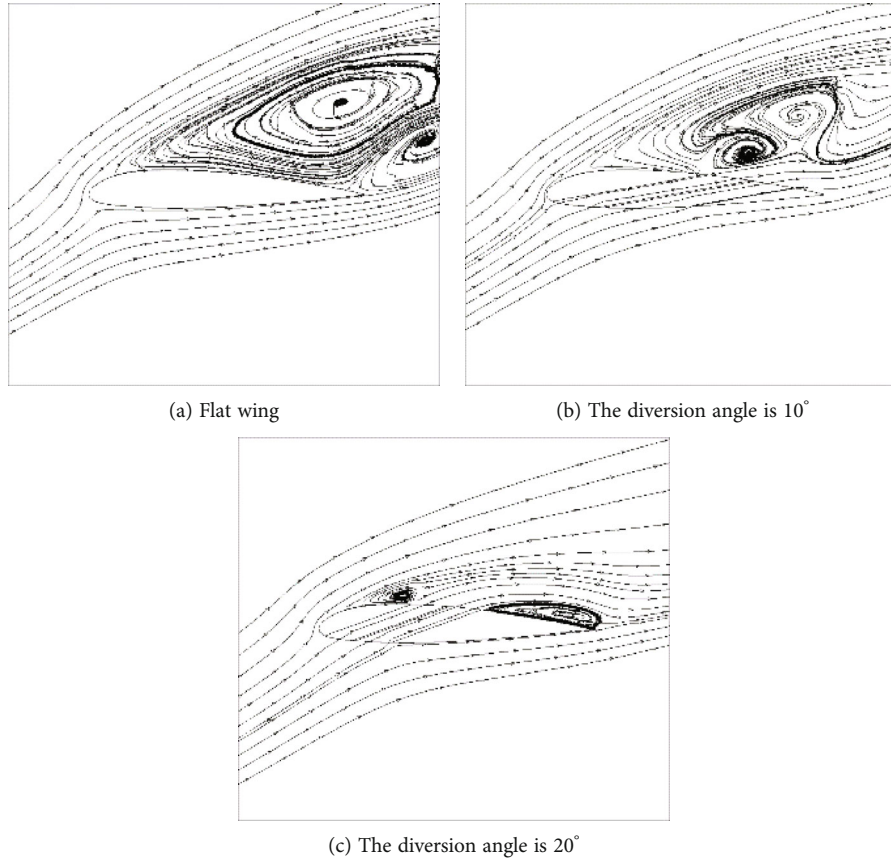(b) The diversion angle is $10°$

(c) The diversion angle is $20°$

FIGURE 20: Fluid streamline diagrams of grid fusion lifting surface with different diversion angle ($Ma = 0.6 \alpha = 28° z/b = 0.75$).

□ Flat wing   △ Grid number = 2
○ Grid number = 1   ☆ Grid number = 3

(a) Lift coefficient curve

□ Flat wing   △ Grid number = 2
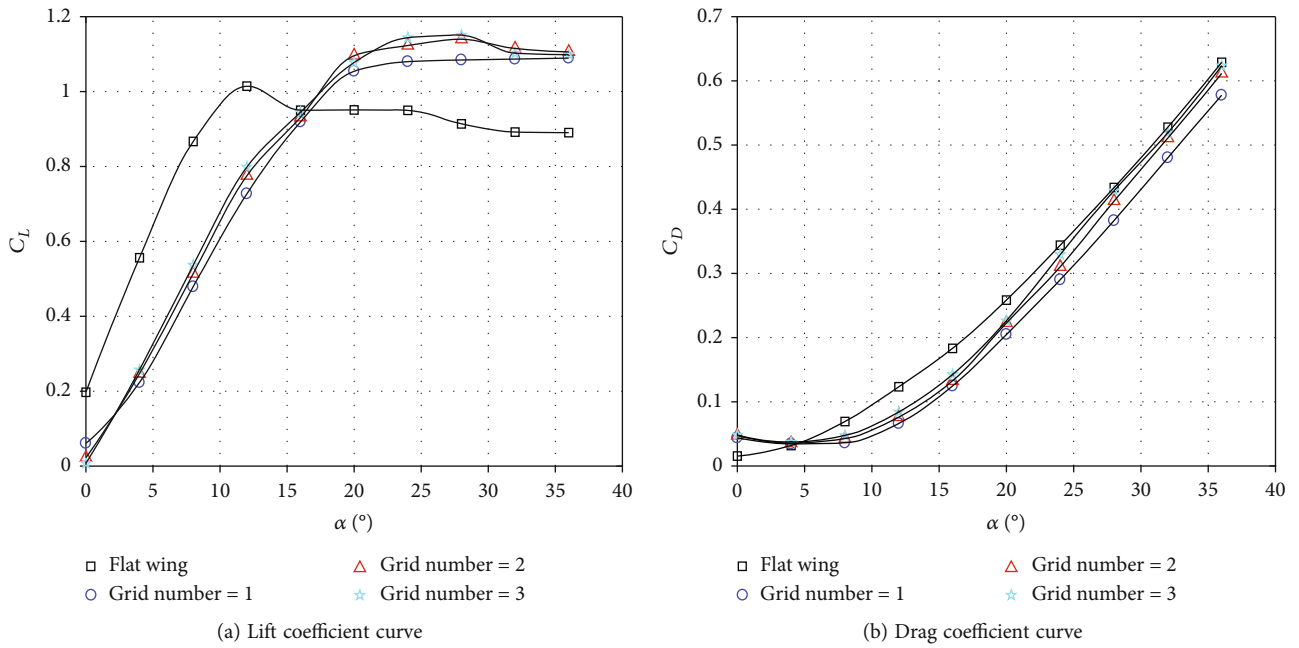○ Grid number = 1   ☆ Grid number = 3

(b) Drag coefficient curve

FIGURE 21: The lift coefficient and drag coefficient curves of the grid fusion lifting surface with different grid numbers ($Ma = 0.6$).

(a) Flat wing

(b) Grid fusion lifting surface with grid number of 1

(c) Grid fusion lifting surface with grid number of 2
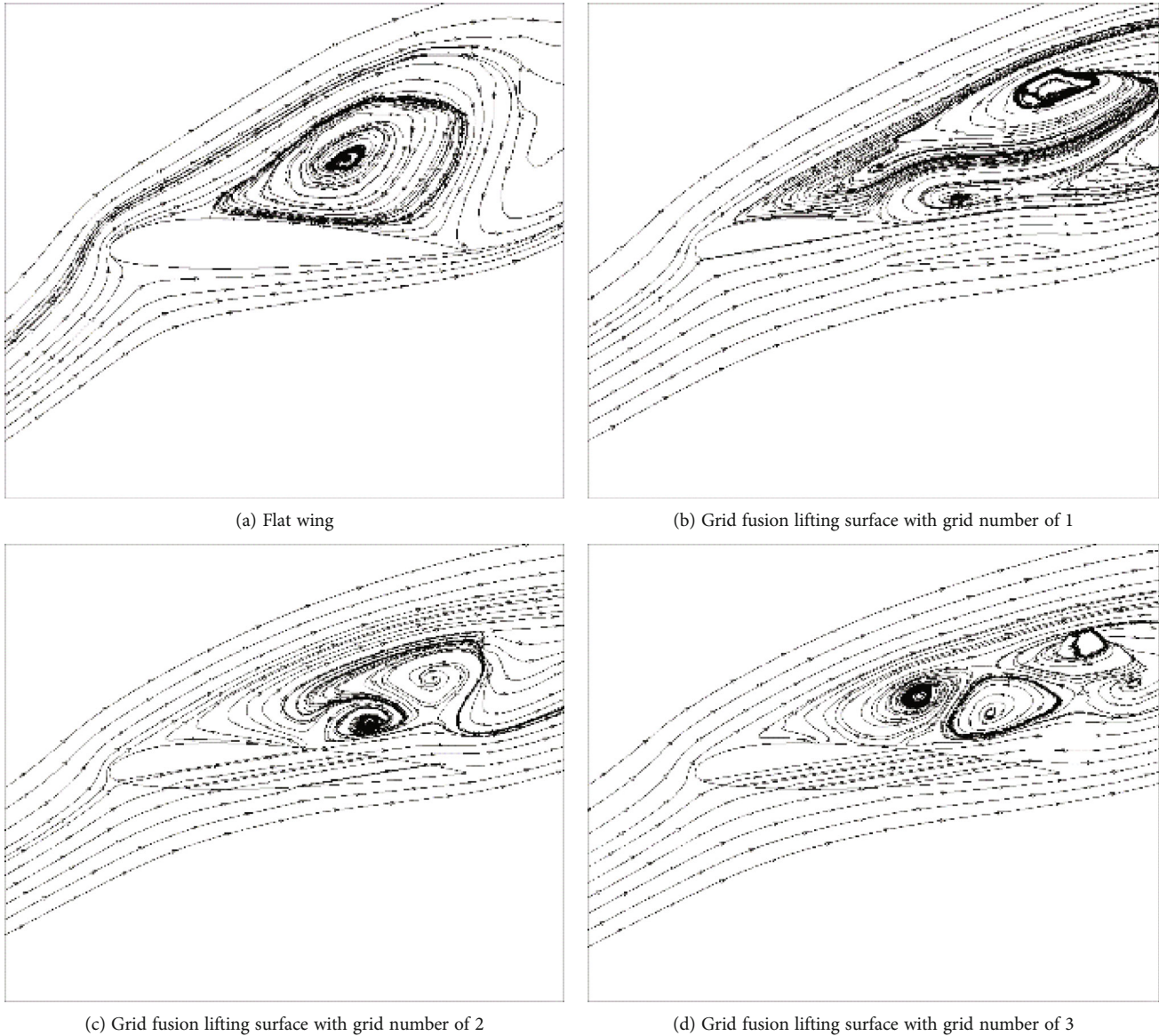
(d) Grid fusion lifting surface with grid number of 3

FIGURE 22: Fluid streamline diagrams of grid fusion lifting surface with different grid numbers ($Ma = 0.6 \alpha = 28° z/b = 0.75$).

lifting surface at a large angle of attack. A smaller grid diversion angle corresponds to a smaller minimum angle of attack to increase the lift force and a wider range of available angles of attack. A larger diversion angle corresponds to a larger stall angle of attack and a larger maximum lift coefficient of the grid fusion lifting surface. During the design of the grid fusion lifting surface aircraft, the corresponding diversion angle can be selected according to different requirements to satisfy the design requirements.

4.4. Influence of the Grid Number on the Aerodynamic Performance of the Grid Fusion Lifting Surface at Large Angles of Attack. Figure 21(a) shows the lift coefficient curve of the grid fusion lifting surface with different grid numbers. The results show that the lift performance of the grid fusion lifting surface is not sensitive to the number of grids under

subsonic conditions and a large angle of attack. The grid fusion lifting surface with a double grid and that with a triple grid do not have greatly different lift coefficients at large angles of attack. Moreover, the grid fusion lifting surface with a single grid has a slightly lower lift coefficient than that with a multigrid at large angles of attack. Figure 21(b) shows the drag coefficient curve of the grid fusion lifting surface with different grid numbers. The results show that the grid fusion lifting surface with different numbers of grids has a slightly smaller drag coefficient than the single wing under subsonic conditions and a large angle of attack. The grid fusion lifting surface with more grids has a slightly greater drag coefficient than that with fewer grids.

Figure 22 shows typical section fluid streamline diagrams of the flat wing and grid fusion lifting surface with different numbers of grids in the subsonic state with an angle of
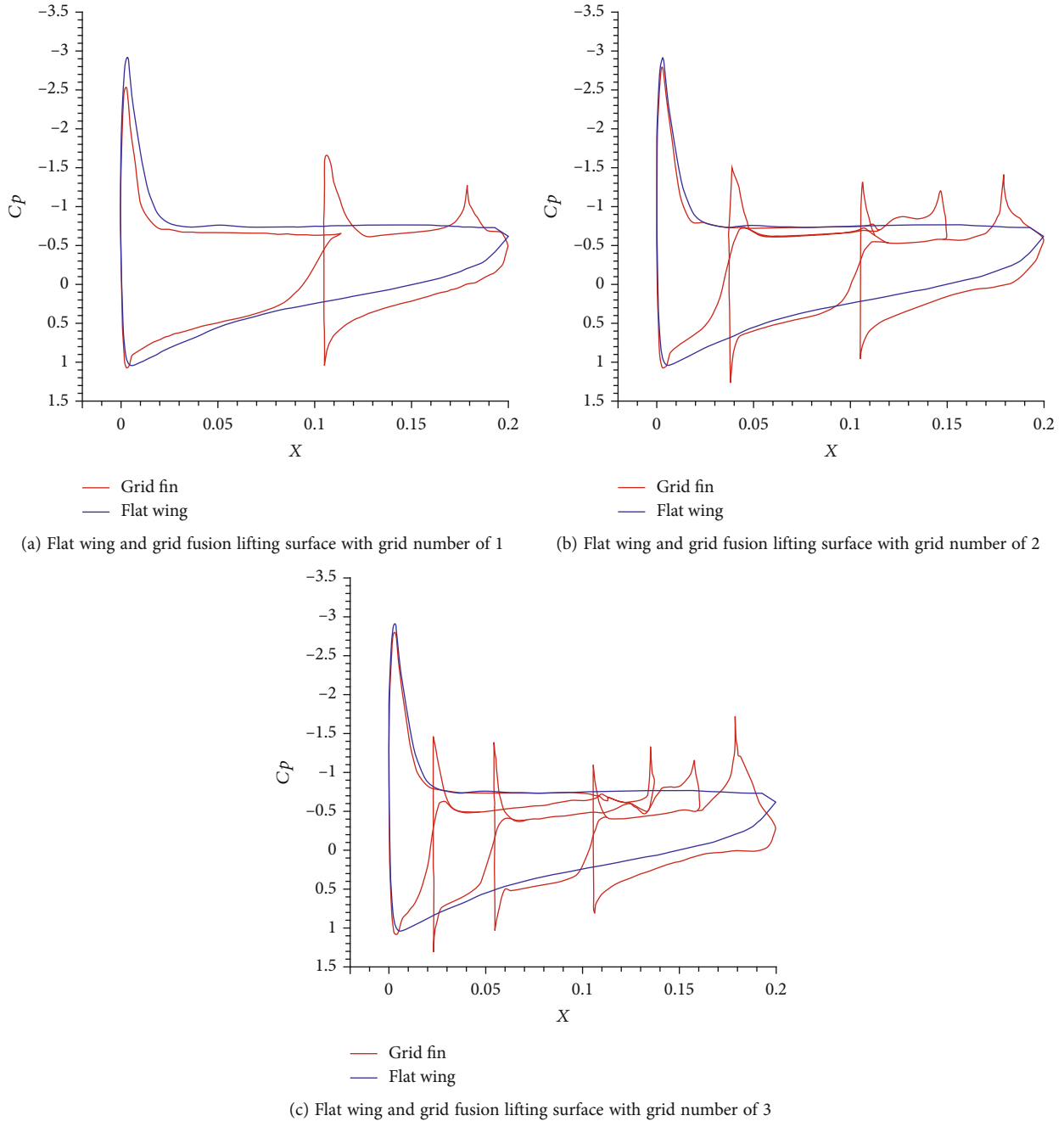
(a) Flat wing and grid fusion lifting surface with grid number of 1

(b) Flat wing and grid fusion lifting surface with grid number of 2

(c) Flat wing and grid fusion lifting surface with grid number of 3

FIGURE 23: Pressure coefficient diagram of flat wing and grid fusion lifting surface with different grid numbers ($Ma = 0.6\,\alpha = 28°\,z/b = 0.75$).

attack of 28°. The results show a minor difference in the airflow separation area on the surface of the grid fusion lifting surface with different grid numbers. Therefore, the number of grids has no substantial effect on the grid fusion lift surface's ability to resist airflow separation for subsonic conditions and large angles of attack.

Figure 23 shows the pressure coefficient diagram of typical sections of the grid fusion lifting surface with different grid numbers in the subsonic state with an angle of attack of 28°. The results show that the pressure distribution in the exposed part of the grid is quite different from that in the grid. Consequently, the ability to generate lift is very dif-

ferent in various grid partition areas. The ability to generate lift force is enhanced because of the increased pressure difference between the upper and lower surfaces of the exposed grid partition. The difference in pressure between the upper and lower surfaces of the grid partitions, which are entirely inside the grid, is small, and the ability to generate lift is weak. With the increase in number of grids, the exposed grid partition area of the grid structure remains unchanged, and the ability to generate lift of the grid partitions inside the grid is weak, so the number of grids hardly affects the lift performance of the grid fusion lifting surface for subsonic flow and large angles of attack.

Increasing the number of grids cannot significantly improve the lift performance of the grid fusion lifting surface at a large angle of attack, but the grid partition inside the grid can generate a specific lift force due to the pressure difference between upper and lower surfaces, so the grid fusion lifting surface with a single grid has a slightly lower lift coefficient than that with more grids.

For subsonic flow and large angles of attack, the number of grids hardly affects the lift performance of the grid fusion lifting surface, so increasing the number of grids has no pronounced effect on improving the lift performance of the grid fusion lifting surface. The grid fusion lifting surface with a single grid has a slightly smaller lift coefficient than that with more grids.

5. Conclusion

Based on the idea of flow control, a type of grid fusion lifting surface suitable for subsonic status and a large angle of attack is designed in this paper. The influence of the grid position, grid diversion angle, and grid number on the aerodynamic performance of the grid fusion lifting surface for subsonic glow and large angles of attack was studied by numerical simulation. The main conclusions are as follows:

(1) The grid fusion lifting surface designed in this paper can effectively improve the lifting performance of the lifting surface under subsonic conditions and a large angle of attack. The stall angle of attack of the front grid fusion lifting surface with a diversion angle of $20°$ increases by $16°$, and the maximum lift coefficient increases by 22.1% compared with the conventional flat wing

(2) The grid position significantly affects the aerodynamic performance of the grid fusion lifting surface under subsonic conditions and a large angle of attack. The front grid fusion lifting surface has larger stall angle of attack and maximum lift coefficient than the flat wing, central grid fusion lifting surface, and rear grid fusion lifting surface under subsonic conditions and a large angle of attack

(3) The effect of the grid diversion angle on the lift performance of the grid fusion lifting surface is more significant under subsonic conditions and a large angle of attack. A smaller grid diversion angle corresponds to a smaller minimum angle of attack to increase the lift force and a wider range of available angle of attack. A larger diversion angle corresponds to a larger stall angle of attack and a larger maximum lift coefficient of the grid fusion lifting surface

(4) The number of grids hardly affects the aerodynamic performance of the grid fusion lifting surface under subsonic conditions and a large angle of attack. The grid fusion lifting surface with a single grid has a slightly worse lift performance than the grid fusion lifting surface with more grids at a large angle of attack

Nomenclature

α: angle of attack
C_L: lift coefficient
C_D: drag coefficient
C_N: normal drag coefficient
C_m: pitching moment coefficient
Cp: pressure coefficient
h: overall grid width
L: reference length
S: reference area
z/b: wing span position.

Data Availability

Some or all data, models, or calculation data in this paper are owned by all the authors, which can be provided with the permission of the authors. Anyone can contact with the corresponding author for further information.

Conflicts of Interest

The authors declare that we have no financial and personal relationships with other people or organizations that can inappropriately influence our work, there is no professional or other personal interest of any nature or kind in any products, service and/or company that could be construed as influencing the position presented in, or the review of, the manuscript entitled.

Acknowledgments

References

[1] T. Lu, X. Wu, J. Lei, and J. Yin, "Numerical study on the aerodynamic coupling effects of spinning and coning motions for a finned vehicle," *Aerospace Science and Technology*, vol. 77, pp. 399–408, 2018.

[2] S. Fan, T. Song, J. Wang, D. Lin, and D. Zheng, "Coupling analysis and dynamic stability boundary of spinning missiles considering actuator dynamics and autopilot," *Aerospace Science and Technology*, vol. 111, article 106481, pp. 1–11, 2021.

[3] F. Wang, J. Liu, H. Qin, Y. Song, L. Chen, and J. Hu, "Unsteady aerodynamic characteristics of slender body at extra-wide angle-of- attack range," *Aerospace Science and Technology*, vol. 110, article 106477, 2021.

[4] C. Berner and A. Dupuis, *Wind Tunnel Tests of a Grid Finned Projectile Configuration*, 2000, AIAA 2000-0105.

[5] J. Despirito, E. V. G. Milton, and W. H. W. David, *CFD Investigation of Canard-Controlled Missile with Planar and Grid Fins in Supersonic Flow*, 2002, AIAA 2002-4509.

[6] S. Chen, M. Khalid, and H. Xu, *A Comprehensive CFD Investigation of Grid Fins as Efficient Control Surface Devices*, 2000, AIAA 2000-0987.

[7] D. C. Raúl, L. Cadarso, and M. Fuentes, "A simplified computational method for two-body high spinning rate vehicles," *Aerospace Science and Technology*, vol. 105, p. 106050, 2020.

[8] S. Chen, M. Khalid, H. Xu, and F. Lesage, "An investigation of the grid fins as control surface devices for missiles," *Aeronautical Journal*, vol. 104, no. 1034, pp. 183–190, 2016.

[9] W. U. Pin, G. M. A. Yong, and C. Chun, "The research analysis of aerodynamic numerical simulation of grid fin," *Journal of Zhejiang University - Science A: Applied Physics & Engineering*, vol. 6, no. 7, pp. 741–746, 2005.

[10] S. S. Chen and F. Deng, "Steady-state computation of roll damping derivatives for missile with grid fins and planar fins," in *Proceedings of 2011 International Conference on Computers, Communications, Control and Automation*, Hongkong, China, 2011.

[11] X. Yang and W. Zhang, "A faster optimization method based on support vector regression for aerodynamic problems," *Advances in Space Research*, vol. 52, no. 6, pp. 1008–1017, 2013.

[12] Y. H. Li, J. X. Shan, J. C. Su, and Y. Huang, "Numerical simulation on circular-arc grid-fin Configurations," *Applied Mechanics and Materials*, vol. 444-445, pp. 342–346, 2013.

[13] C. D. Huang, W. Liu, and G. W. Yang, "Numerical studies of static aeroelastic effects on grid fin aerodynamic performances," *Chinese Journal of Aeronautics*, vol. 30, no. 4, pp. 1300–1314, 2017.

[14] Y. C. Liu, Z. X. Xia, and J. Liu, "Numerical simulation of aerodynamic characteristics and heating for grid fin missiles," *Proceedings of the Institution of Mechanical Engineers, Part G: Journal of Aerospace Engineering*, vol. 233, no. 7, pp. 2368–2377, 2019.

[15] M. Tripathi, M. M. Sucheendran, and A. Misra, "Effect of aspect ratio variation on subsonic aerodynamics of cascade type grid fin at different gap-to-chord ratios," *Aeronautical Journal*, vol. 124, no. 1274, pp. 472–498, 2020.

[16] P. Dehghani and M. Mahdi, "Numerical analysis of the effect of sweep-back angle on the stability derivatives of the grid fin," *Journal of the Brazilian Society of Mechanical Sciences and Engineering*, vol. 41, no. 7, pp. 1–13, 2019.

[17] D. S. James, E. Milton, and J. Vaughn, *Subsonic flow CFD investigation of canard controlled missile with planar and grid fins*, 2003, AIAA-2003-500.

[18] D. A. Pruzan and M. R. Mendenhall, *Grid fin stabilization of the orion launch abort vehicle*, 2011, AIAA-2011-3018.

[19] J. Allen and M. Ghoreyshi, "Forced motions design for aerodynamic identification and modeling of a generic missile configuration," *Aerospace Science and Technology*, vol. 77, pp. 742–754, 2018.

[20] H. Li and Z. Y. Ye, "Numerical investigation on aerodynamic and inertial couplings of flexible spinning missile with large slenderness ratio," *Aerospace Science and Technology*, vol. 99, p. 105582, 2020.

[21] M. Debiasi, Z. Yan, and C. T. Loon, "Swept-back grid fins for transonic drag reduction," in *28th AIAA Applied Aerodynamics Conference*, Chicago, Maryland, 2010.

[22] J. Cai, "Numerical study on choked flow over grid-fin configurations," *Journal of Spacecraft and Rockets*, vol. 46, no. 5, pp. 949–956, 2009.

[23] F. Bouquet, J. A. Wildschut, and H. C. Hakkesteegt, "Experimental study of stagnation pressure reaction control for midcalibre non-spinning projectiles," *Aerospace Science and Technology*, vol. 110, p. 106449, 2021.

[24] Q. M. Chen, T. X. Hu, P. Q. Liu, Q. Qu, H. Guo, and R. A. D. Akkermans, "The dynamic vortical flow behaviour on a coplanar canard configuration during large-amplitude-pitching," *Aerospace Science and Technology*, vol. 112, p. 106553, 2021.

[25] P. J. Attar, R. E. Gordnier, and M. R. Visbal, "Numerical simulation of full-span delta wing buffet at high angle of Attack," *Journal of Aircraft*, vol. 45, no. 3, pp. 857–867, 2008.

[26] J. Zhang, Y. Ai, D. Huang, and J. Liu, "Numerical simulation investigation of aerodynamic interference of sting support in wind tunnel test of a delta wing at big angels of attack," *Acta Aeronautica et Astronautica Sinica*, vol. 37, no. 8, pp. 2481–2489, 2016.

[27] J. E. Burkhalter and H. M. Frank, "Grid fin aerodynamics for missile applications in subsonic flow," *Journal of Spacecraft and Rockets*, vol. 33, no. 1, pp. 38–44, 1996.